

## High-resolution photoabsorption measurement and multichannel quantum-defect-theory analysis of the $2p^5 3s(^1P_1) ns, nd$ autoionizing series of sodium

M. A. Baig

*Atomic and Molecular Physics Laboratory, Department of Physics, Quaid-I-Azam University, Islamabad, Pakistan*

S. A. Bhatti

*Applied Physics Division, PINSTECH, P. O. Box Nilore, Islamabad, Pakistan*

(Received 22 November 1993)

We measured the photoabsorption spectrum of sodium in the  $2p$  subshell excitation region using synchrotron radiation and a 3-m spectrograph at a resolution of  $\pm 0.008 \text{ \AA}$ . In spite of the large number of overlapping structure due to the four ionization limits  $2p^5 3s(^3P_{210})$  and  $^1P_1$ , well separated autoionizing Rydberg series are detected converging to the  $2p^5 3s(^1P_1)$  threshold. A three-channel quantum-defect-theory analysis is performed for the  $2p^5 3s(^1P_1) ns$  and  $2p^5 3s(^1P_1) nd$  autoionizing resonances. A simple  $n$ -channel multichannel quantum-defect-theory formula in terms of cofactors is presented for the calculation of the photoionization cross section for one open and  $(n-1)$  bound channels.

PACS number(s): 32.30.Jc, 32.70.Jz, 32.80.Dz, 32.80.Fb

The  $2p$  inner-shell excitation in sodium leads to four ionic states  $2p^5 3s(^3P_{210})$  and  $^1P_1$  which serve as series limits for the Rydberg series according to the dipole-allowed photoabsorption from the  $2p^6 3s(^2S_{1/2})$  ground state. Accordingly, there are four groups of Rydberg series converging on these pertinent ionic levels: four Rydberg series  $2p^5 3s(^3P_2) ns [2]_{3/2}^0$ ,  $nd[0]_{1/2}^0$ ,  $nd[1]_{1/2,3/2}^0$  and  $nd[2]_{3/2}^0$  to the  $2p^5 3s(^3P_2)$  limit at  $306\,377.65 \text{ cm}^{-1}$ , three series  $2p^5 3s(^3P_1) ns[1]_{1/2,3/2}^0$ ,  $nd[1]_{1/2,3/2}^0$ ,  $nd[2]_{3/2}^0$  to the  $2p^5 3s(^3P_1)$  limit at  $307\,142.94 \text{ cm}^{-1}$ , two series  $2p^5 3s(^3P_0) ns[0]_{1/2}^0$ ,  $nd[2]_{3/2}^0$  to the  $2p^5 3s(^3P_0)$  limit at  $307\,735.01 \text{ cm}^{-1}$ , and three series  $2p^5 3s(^1P_1) ns[1]_{1/2,3/2}^0$ ,  $nd[1]_{1/2,3/2}^0$ , and  $nd[2]_{3/2}^0$  to the  $2p^5 3s(^1P_1)$  limit at  $310\,216.32 \text{ cm}^{-1}$ . Due to the small spin-orbit interaction parameter  $\xi_p = 980 \text{ cm}^{-1}$  in the  $2p^5 3s$  parent-ion configuration, the  $^3P$  fine-structure levels lie very close in energy, whereas the  $^1P$  level lies about  $2481 \text{ cm}^{-1}$  above the triplet levels. Consequently, the Rydberg series to the  $^1P$  limit are well isolated in energy from the series to the  $^3P$  limits. Indeed we have observed strong Rydberg series of  $ns$  and  $nd$  character to the  $2p^5 3s(^1P_1)$  limit and very weak series to all the  $2p^5 3s(^3P_{210})$  limits. Since all the observed transitions lie above the first ionization threshold, they can decay into the underlying  $2p^6 \epsilon p$  continuum; as a result, the lines show Beutler-Fano- [1] type autoionizing resonances. We have observed the strongly autoionizing Rydberg series  $2p^5 3s(^1P_1) nd$  up to  $n=20$ . The  $2p^5 3s(^1P_1) ns$  series can be resolved from the  $nd$  series up to  $n=15$ , a considerable extension from the previous observation of these series up to  $n=10$  and  $5$ , respectively [2,3].

In this paper we present the analysis of the autoionizing  $2p^5 3s(^1P_1) nd$  and  $2p^5 3s(^1P_1) ns$  resonances to the  $2p^5 3s(^1P_1)$  limit based on the phase-shifted reaction-matrix multichannel quantum-defect theory (MQDT) of Cooke and Cromer [4] and Giusti-Suzor and Fano [5]. We also present a simple  $n$ -channel MQDT expression in terms of cofactors to calculate the photoionization cross section for the case of one open and  $(n-1)$  bound chan-

nels. The existing relations for calculating the photoionization cross section for one open and one bound channel [5] and one open and two bound channels [6–8] are derived from the general MQDT formula.

The spectra were recorded in the first order of a 3-m vacuum spectrograph equipped with a 5000-line/mm holographic grating. The equipment is capable of delivering a resolution of the order of  $0.008 \text{ \AA}$  with a  $10\text{-}\mu\text{m}$  slit width and the reciprocal dispersion is  $0.66 \text{ \AA/mm}$  at  $400 \text{ \AA}$ . Synchrotron radiation emitted from the 500-MeV electron accelerator provided the background source of continuum. An absorption column approximately  $1000 \text{ mm}$  long was achieved by vaporizing metallic sodium in a resistively heated furnace of inner diameter  $2 \text{ cm}$  and  $1 \text{ mm}$  wall thickness. The furnace was operated at temperatures in the range of  $350\text{--}450^\circ\text{C}$ , which correspond to vapor pressure of sodium about  $0.3$  to  $1 \text{ Torr}$ , respectively. The spectra were calibrated in energy by superposing the absorption spectra of helium [9] and neon [10], both of which contain well-distributed lines in the spectral region investigated in the present experiment.

The spectra were recorded on Kodak SWR plates with exposure times ranging from  $5$  to  $10 \text{ min}$ . The plates were measured on an Abbe comparator with an absolute accuracy of  $\pm 0.008 \text{ \AA}$  for sharp lines. The dispersion curve was fitted by a third-order Chebyshev polynomial to an internal consistency of  $\pm 0.002 \text{ \AA}$ . The spectra recorded on the photographic plates were digitized with a computer-controlled microdensitometer in steps of  $5 \mu\text{m}$  using a slit width of  $10 \mu\text{m}$  at the photomultiplier.

A densitometer trace of the photoabsorption spectrum is presented in Fig. 1, which shows the overlapping structure of Rydberg series in the vicinity of the four series limits, marked as arrows. The observed Rydberg series to the  $2p^5 3s(^1P_1)$  singlet-based limit are well developed, whereas the series to the  $2p^5 3s(^3P_{210})$  triplet-based limits are too weak to be detected near the limits. The striking feature of the observed  $2p^5 3s(^1P_1) ns$  and  $nd$  series is that

the  $nd$  lines have broad, typical Beutler-Fano profiles, whereas the  $ns$  lines are relatively sharp, a close similarity with the autoionizing Rydberg series observed in inert gases [10–15], where the  $mp^5(^2P_{1/2})$  ( $m=2, 3, 4$ , and 5 for neon, argon, krypton, and xenon, respectively) based  $nd[3/2]_1$  series show autoionization and the  $ns[1/2]_1$  series remain sharp. Another interesting observation is that the  $2p^53s(^1P_1)6d$  line, which lies just above the  $2p^53s(^3P_2)$  limit, shows pronounced autoionization effect, whereas the adjacent lower member of this series  $2p^53s(^1P_1)5d$ , which lies below the  $2p^53s(^3P_2)$  limit, exhibits very strong and sharp resonance. The  $2p^53s(^1P_1)7s$  line also shows some broadening effects but it remains relatively sharp (see Fig. 1). This abrupt change in the line shapes of the  $nd$ -series members across the  $2p^53s(^3P_2)$  limit indicates that the  $2p^53s(^1P_1)nd$  bound channel is strongly coupled to the  $2p^53s(^3P_2)\epsilon l$  open channel and only weakly coupled to the  $2p^6(^1S_0)\epsilon p$  open channel. The coupling of the  $2p^53s(^1P_1)ns$  series members to the  $2p^53s(^3P_2)\epsilon l$  open channel is small and, consequently, the lines of the  $2p^53s(^1P_1)ns$  Rydberg series remain sharp.

In order to analyze the line shapes of the observed autoionizing resonances, we have used the phase-shifted multichannel quantum-defect theory reaction-matrix formalism as given by Cooke and Cromer [4]. The MQDT equation takes a matrix form

$$[\mathbf{R} + \boldsymbol{\epsilon}]\mathbf{a} = 0, \quad (1)$$

where  $\mathbf{R}$  is the interaction matrix whose diagonal elements are zero, the off-diagonal elements  $R_{ij}$  describe the interaction between the  $i$ th and  $j$ th channels, and  $\boldsymbol{\epsilon}$  is the diagonal matrix whose components for the bound channels are given as

$$\epsilon_i = \tan[\pi(\nu_i + \mu_i)], \quad (2)$$

where  $\mu_i$  is the quantum defect,  $\nu_i$  is the effective quantum number of the  $i$ th bound channel with respect to the  $i$ th ionization threshold,  $\nu_i = [\mathbf{Ry}/(I_i - E_n)]^{1/2}$ , and  $\mathbf{a}$  is

the column vector given as

$$a_i = A_i \cos[\pi(\nu_i + \mu_i)], \quad (3)$$

where  $A_i$  are the amplitudes of the  $i$ th dissociation channel. For the open channels  $\epsilon_{ij}$  are the phase shifts which are equal to  $\epsilon_0$  and  $\mathbf{a}$  is normalized such that

$$\sum_0 a_0^2 = [1 + \epsilon_0^2]^{-1}. \quad (4)$$

In the autoionization region the atomic spectra can be well described by one generalized continuum and  $(n-1)$  bound channels. The MQDT compatibility equation takes a particularly simple form:

$$\begin{pmatrix} \epsilon_1 & R_{12} & R_{13} & \cdots & R_{1n} \\ R_{12} & \epsilon_2 & R_{23} & & R_{2n} \\ R_{13} & R_{23} & \epsilon_3 & & R_{3n} \\ & & & & \epsilon_n \\ R_{1n} & R_{2n} & R_{3n} & & \epsilon_n \end{pmatrix} \begin{pmatrix} a_1 \\ a_2 \\ a_3 \\ \vdots \\ a_n \end{pmatrix} = 0. \quad (5)$$

Considering channel 1 open and channels from 2 to  $n$  as bound, a nontrivial solution of the MQDT equation (5) requires the determinant of the coefficient matrix to vanish. The determinant is equal to

$$\epsilon_1 C_{11} + \sum_2^n R_{1i} C_{1i} = 0. \quad (6)$$

Here the determinant has been expanded by the first row and the summation is over the bound channels. The  $C_{1i}$  are the cofactors of the first row of the MQDT matrix. This immediately yields

$$\epsilon_1 = -(1/C_{11}) \sum_2^n R_{1i} C_{1i}. \quad (7)$$

Substituting it in the normalization condition for the open channel,  $a_1^2 = [1 + \epsilon_1^2]^{-1}$ , it yields

$$a_1^2 = C_{11}^2 / C_{11}^2 + \left| \sum_2^n R_{1i} C_{1i} \right|^2. \quad (8)$$

The next step is to write the last  $(n-1)$  equations in the matrix form

$$\begin{pmatrix} \epsilon_2 & R_{23} & \cdots & R_{2n} \\ R_{23} & \epsilon_3 & & R_{3n} \\ & & & \epsilon_n \\ R_{2n} & R_{3n} & & \epsilon_n \end{pmatrix} \begin{pmatrix} a_2/a_1 \\ a_3/a_1 \\ \vdots \\ a_n/a_1 \end{pmatrix} = - \begin{pmatrix} R_{12} \\ R_{13} \\ \vdots \\ R_{1n} \end{pmatrix}. \quad (9)$$

The quantities we will need are the square of the ratio of the amplitudes in the dissociation channels. All the  $(a_i/a_1)$  can be calculated from the above relation using the Cramer's rule for solving the set of simultaneous inhomogeneous equations:

$$a_i/a_1 = -C_{1i}/C_{11}. \quad (10)$$

The denominator determinant is the cofactor  $C_{11}$ , while the numerator is the cofactor  $C_{1i}$  with the negative sign.

The photoionization cross section is calculated using the expression [4–7]

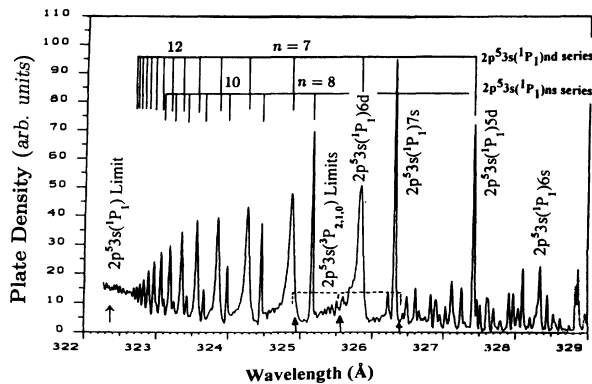


FIG. 1. The densitometer trace of the photoabsorption spectrum of sodium in the region between 290–320 Å showing overlapping Rydberg series to all the four limits of the  $2p^53s$  parent-ion configuration. The ionization thresholds  $2p^53s(^3P_{210})$  and  $^1P_1$  are labeled as arrows. The change in the linewidth of the  $2p^53s(^1P_1)5d$  and the adjacent member  $2p^53s(^1P_1)6d$  is quite evident across the  $2p^53s(^3P_2)$  threshold.

$$\sigma = K \left| \sum_1^n a_i D_i \right|^2, \quad (11)$$

where  $K = 4\pi^2 \alpha \hbar \omega$  which does not change appreciatively over the energy range covered by a typical single-photon autoionizing spectra. Here  $\hbar \omega$  is the photon energy and  $\alpha$  is the fine-structure constant. The short-range parameters  $D_i$  are the transition dipole moments between the initial state and the  $i$ th channel. Substituting the values of  $a_i$  in this equation, the photoionization cross section can be expressed as

$$\sigma = K (a_1^2 / C_{11}^2) \left| \sum_1^n C_{1i} D_i \right|^2. \quad (12)$$

Incorporating the value of the  $a_1^2$  from Eq. (8) in the above relation, a generalized expression for the photoionization cross section with one open and  $(n-1)$  bound channels is obtained:

$$\sigma = K \left| \sum_1^n C_{1i} D_i \right|^2 / C_{11}^2 + \left| \sum_2^n C_{1i} R_{1i} \right|^2. \quad (13)$$

Note that the summation in the numerator is over all the  $n$  channels involved, while in the denominator the summation is only over the  $(n-1)$  bound channels.

From this general expression, we can derive the existing relations [4,5] to calculate the photoionization cross section. The simplest case is with one open and one bound channel. The MQDT matrix for this situation is

$$\sigma = K \frac{|(\epsilon_2 \epsilon_3 - R_{23}^2) D_1 - (\epsilon_3 R_{12} - R_{13} R_{23}) D_2 - (\epsilon_2 R_{13} - R_{12} R_{23}) D_3|^2}{(\epsilon_2 \epsilon_3 - R_{23}^2)^2 + |(\epsilon_2 R_{13}^2 + \epsilon_3 R_{12}^2 - 2R_{12} R_{13} R_{23})|^2}. \quad (18)$$

This expression is identical to but much simpler than the relation derived by Giusti-Suzor and Lefebvre-Brion [6], Ueda [7], and Hieronymus, Neukammer, and Rinneberg [8]. One can similarly write the expressions for the  $(n-1)$  bound channels interacting with one open channel. The main advantage of the general expression for calculating the photoionization cross section in terms of cofactors [Eq. (13)] is that the computer code remains as simple as for the one open and one bound channel problem.

For the quantitative analysis of the observed autoionizing resonances, the generalized quantum-defect-theory expression (13) was used for three channels. The open channel is  $2p^5 3s(^3P_2)\epsilon l$  and the two bound channels are  $2p^5 3s(^1P_1)ns$  and  $2p^5 3s(^1P_1)nd$ , respectively. There also exists the  $2p^6(^1S_0)\epsilon p$  open channel which should be taken into account for the MQDT analysis. However, the energy difference between the  $2p^6(^1S_0)$  threshold and the  $2p$  inner-shell excitation structure is about 30 eV; therefore, its contribution can be neglected. Furthermore, there is no observed background due to the direct excitation in the  $2p^6(^1S_0)\epsilon p$  continuum channel (see Fig. 1). The two Rydberg series  $2p^5 3s(^1P_1)ns$  and  $2p^5 3s(^1P_1)nd$  both terminate to the same ionization threshold; thus,  $I_2 = I_3 = 310\,212.2 \text{ cm}^{-1}$ . The quantum defects calculated with respect to the ionization limit are  $0.618 \pm 0.008$  and  $0.275 \pm 0.008$  for the  $ns$  and the  $nd$  series, respectively,

$$\begin{pmatrix} \epsilon_1 & R_{12} \\ R_{12} & \epsilon_2 \end{pmatrix}, \quad (14)$$

where  $\epsilon_2 = \tan[\pi(\nu_2 + \mu_2)]$ . The cofactors of the first row are  $C_{11} = \epsilon_2$  and  $C_{12} = -R_{12}$ . Substituting these values in the expression (13), the relation for the photoionization cross section becomes

$$\sigma = K \frac{|\tan[\pi(\nu_2 + \mu_2)] D_1 - R_{12} D_2|^2}{\tan^2[\pi(\nu_2 + \mu_2)] + R_{12}^4}. \quad (15)$$

This is the same expression as derived by Giusti-Suzor and Fano [5] and Cooke and Cromer [4].

For the three-channel problem, one open and two bound channels, the MQDT matrix is

$$\begin{pmatrix} \epsilon_1 & R_{12} & R_{13} \\ R_{12} & \epsilon_2 & R_{23} \\ R_{13} & R_{23} & \epsilon_3 \end{pmatrix}, \quad (16)$$

where  $\epsilon_2 = \tan[\pi(\nu_2 + \mu_2)]$  and  $\epsilon_3 = \tan[\pi(\nu_3 + \mu_3)]$ . The cofactors of the first row are

$$\begin{aligned} C_{11} &= (\epsilon_2 \epsilon_3 - R_{23}^2), & C_{12} &= -(\epsilon_3 R_{12} - R_{13} R_{23}), \\ C_{13} &= -(\epsilon_2 R_{13} - R_{12} R_{23}). \end{aligned} \quad (17)$$

The photoionization cross-section expression in this case becomes

which remain nearly constant, an indication of a negligible interchannel interaction among these bound channels; thus, we put  $R_{23} = 0$ .

The results of our calculations are presented in Fig. 2. The upper curve shows the calculated spectrum with the parameters given in Table I and the lower curve shows the experimentally observed spectrum. We have used the experimental bandwidth of about  $5 \text{ cm}^{-1}$  for averaging the calculated data. The calculated spectrum shows a remarkable reproduction of the experimental spectrum and demonstrates the power of the MQDT to analyze the autoionizing resonances.

From the parameters in Table I it can be seen that the coupling of the  $2p^5 3s(^1P_1)nd$  series to the  $2p^5 3s(^3P_2)\epsilon l$  open channel is nearly three times stronger than that of the  $2p^5 3s(^1P_1)ns$  series. The observed widths (full width at half maximum) of the  $2p^5 3s(^1P_1)6d$  resonance at  $325.8 \text{ \AA}$  ( $110 \pm 10 \text{ cm}^{-1}$ ) and that of the  $2p^5 3s(^1P_1)7s$  resonance at  $326.3 \text{ \AA}$  ( $40 \pm 10 \text{ cm}^{-1}$ ) also follow a similar trend. These parameters can be extended in the discrete region, below the  $2p^5 3s(^3P_2)$  threshold by using the Lu-Fano graphical technique [16] as has been done in barium [17]. There are at least 12 possible overlapping Rydberg series in this region: three  $nd$  and one  $ns$  series built on the  $2p^5 3s(^3P_2)$  limit, two  $nd$  and one  $ns$  series built on the  $2p^5 3s(^3P_1)$  limit, one  $nd$  and one  $ns$  series built on the  $2p^5 3s(^3P_0)$  limit, and two  $nd$  and one  $ns$  series built on

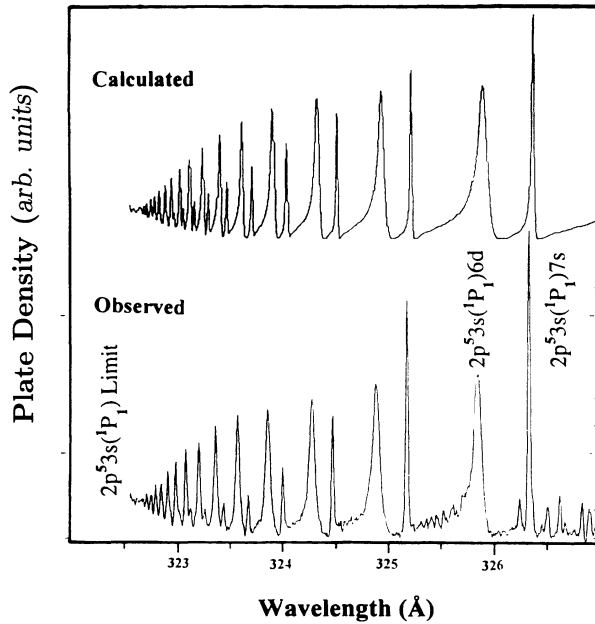


FIG. 2. The calculated and the observed  $2p^5 3s(^1P_1)ns, nd$  series of autoionizing resonances in the absorption spectrum of sodium covering the spectral region between 322–327 Å. The MQDT parameters used to reproduce the observed structure are listed in Table I. An experimental bandwidth of  $5 \text{ cm}^{-1}$  was used to average the calculated spectra in order to match the observed spectrum.

the  $2p^5 3s(^1P_1)$  limit, within the framework of the  $J_c K$ -coupling scheme [18,19]. The interchannel interactions among these overlapping resonances seems to perturb the spectrum. In order to extract some meaningful parameters and a reliable interpretation, one must include all these channels in the MQDT analysis. We have not been able to perform this extensive analysis because of the weak nature of the observed structure in this region. A reinvestigation of this part of the spectrum at a higher dispersion and resolution will be very beneficial for extending the MQDT analysis.

In the inert gases, the  $(^2P_{1/2})nd[3/2]_1$  series shows Beutler-Fano-type autoionizing resonances because the  $K$  quantum number in the  $(^2P_{3/2})\epsilon d[3/2]_1$  continuum

TABLE I. Three-channel MQDT parameters for the analysis of the autoionizing  $2p^5 3s(^1P_1)ns, nd$  Rydberg series in sodium.

$i, j$	1	2	3
$ i\rangle$	$2p^5 3s(^3P_2)\epsilon l$	$2p^5 3s(^1P_1)ns$ $R_{12}=0.13$	$2p^5 3s(^1P_1)nd$ $R_{13}=0.35$ $R_{23}=0$
$\mu_i$	0	0.618	0.275
$D_i$	-3.0	2.2	4
$I_i$	$306\,377.6 \text{ cm}^{-1}$	$310\,212.2 \text{ cm}^{-1}$	$310\,212.2 \text{ cm}^{-1}$

channel and the discrete channel is identical. The  $(^2P_{1/2})ns[1/2]_1$  series remains sharp because the  $K$  quantum numbers differ in the discrete and the  $(^2P_{3/2})\epsilon s[3/2]_1$  continuum channels. The situation in sodium is more complicated due to the existence of four thresholds as a result of the fine-structure splitting in the  $2p^5 3s$  parent-ion configuration. An analogous analysis, therefore, cannot be extended for the interpretation of the autoionization in the  $2p^5 3s(^1P_1)nd$  series in sodium because numerous open channels  $2p^5 3s(^3P_{2,1,0})\epsilon s$  and  $\epsilon d$  possessing  $K=[1]_{1/2,3/2}$  and  $[2]_{3/2}$  are present which can cause autoionization for both the  $2p^5 3s(^1P_1)nd[1]_{1/2,3/2}$  and the  $2p^5 3s(^3P_1)ns[1]_{1/2,3/2}$  series. The reason only the  $2p^5 3s(^1P_1)nd$  series is broadened and the  $2p^5 3s(^1P_1)ns$  series remains relatively sharp is not clear.

In conclusion, we have demonstrated that the  $2p^5 3s(^1P_1)nd$  and  $2p^5 3s(^1P_1)ns$  autoionizing resonances observed in the photoabsorption spectrum of sodium in the  $2p$ -subshell excitation region show remarkable similarity to that of the autoionizing resonances  $mp^5(^2P_{1/2})nd[3/2]_1$  and  $ns[3/2]_1$  in inert gases. The observed overlapping series of autoionizing resonances have been parametrized using a three-channel quantum-defect-theory approach, one open and two bound channels. A simple  $n$ -channel MQDT relation in terms of cofactors is presented to calculate the photoionization cross section for one open and  $(n-1)$  bound channels. As the generalized expression is derived in terms of cofactors, the computer code for a higher number of interacting channels remains practically the same and runs almost as fast as for the two or three interacting channels model.

[1] U. Fano, Phys. Rev. **124**, 1866 (1961).  
 [2] J. P. Connerade *et al.*, Astro. Phys. J. **165**, 203 (1971).  
 [3] H. Wolf *et al.*, Z. Phys. **252**, 353 (1972).  
 [4] W. E. Cooke and C. L. Cromer, Phys. Rev. A **32**, 2725 (1984).  
 [5] A. Giusti-Suzor and U. Fano, J. Phys. B **17**, 215 (1984).  
 [6] A. Giusti-Suzor and H. Lefebvre-Brion, Phys. Rev. A **30**, 3057 (1984).  
 [7] K. Ueda, Phys. Rev. A **35**, 2484 (1987).  
 [8] H. Hieronymus *et al.*, J. Phys. B **25**, 3463 (1992).  
 [9] M. A. Baig *et al.*, J. Phys. B **17**, L271 (1984).  
 [10] M. A. Baig and J. P. Connerade, J. Phys. B **17**, 1785 (1984).

[11] M. A. Baig, J. P. Connerade, and M. Pantelorous (unpublished).  
 [12] K. Yoshino, J. Opt. Soc. Am. **60**, 536 (1970).  
 [13] K. Yoshino and Y. Tanaka, J. Opt. Soc. Am. **69**, 159 (1979).  
 [14] R. D. Bonin *et al.*, J. Opt. Soc. Am. B **2**, 1275 (1985).  
 [15] K. Ito *et al.*, J. Opt. Soc. Am. B **5**, 2006 (1988).  
 [16] K. T. Lu and U. Fano, Phys. Rev. A **2**, 81 (1970).  
 [17] C. J. Dai *et al.*, J. Opt. Soc. Am. B **6**, 1486 (1989).  
 [18] G. Racah, Phys. Rev. **61**, 546 (1942).  
 [19] R. D. Cowan, *The Theory of Atomic Structure and Spectra* (University of California Press, Berkeley, 1981).